Prioritizing mitigation efforts for intra-urban heat vulnerability using a case study of San Antonio, Texas

Author list:

Kristen E. Brown*, Wei Zhai, Esteban A. López Ochoa

Declarations

All authors contributed to the study conception and design. Material preparation, data collection, and analysis were performed by Kristen E Brown and Wei Zhai. The first draft of the manuscript was written by Kristen E Brown and all authors commented on the manuscript. All authors read and approved the final manuscript.

Funding

This work was supported by the City of San Antonio.

Disclosure

The authors report there are no competing interests to declare.

Data Availability Statement

The data that support the findings of this study were derived from the following resources available in the public domain:

Landsat U.S. Analysis Ready Data at https://doi.org/10.5066/P960F8OC

PLACES: Local Data for Better Health, Census Tract Data 2023 release at https://data.cdc.gov/500-Cities-Places/PLACES-Local-Data-for-Better-Health-Census-Tract-D/em5e-5hvn/about_data

The US Census Bureau https://www.census.gov/data.html

World Urban Database and Access Portal Tools https://www.wudapt.org/

Due to the sensitive nature of the data, energy burden data is not available.

Abstract

Many urban areas, particularly in the southern United States (US), experience extreme heat causing discomfort and illness. Heat vulnerability is not uniform across a city due to the built-environment and socioeconomic conditions, impacting some areas more than others. Therefore, it is important that heat reduction actions prioritize areas that are most vulnerable. To help ensure mitigation and adaptation efforts are most effectively targeted, analytical techniques are used to quantify vulnerability to heat. A case study of Bexar County, home to San Antonio, Texas, is used to demonstrate identification of vulnerability using high resolution land surface temperature (LST) data from the Landsat program and socio-economic data from the US Census Bureau and American Community Survey. The index is validated using chronic disease information from CDC Places as well as energy burden data. Specific heat mitigation measures may be best sited through consideration of additional variables, including characteristics of the built environment. An analysis of vulnerability by local climate zone (LCZ) is performed.

Keywords

Urban areas; Climate Change; Exposure Parameters; Temperature; Sustainable Development

Introduction

Exposure to extreme heat in urban areas is concerning, due to its adverse effects on human wellbeing and health. There is a strong association with increased mortality during heat events for those living alone, confined to bed, unable to care for themselves, unable to access a cooler location, and with pre-existing health conditions (Khatana et al. 2022). It is critical to identify where the most intense temperatures occur and to explore whether the people in these areas have resources to cope with the impacts (Georgescu et al. 2024). An individual's response to an environmental stressor is a function of (1) the presence of the threat and (2) the person's ability to avoid the stressor, requiring consideration of the quality of the environment (or presence of threats) while acknowledging that environmental burdens are not borne equally, even within the same physical space. Growing urban communities sustainably demands a data-driven process to support policy decisions in the interest of equity and environmental justice. It is essential to capture interactions between urban environmental systems and human behaviors and the effect that socio-economic drivers have on these interactions. Prior research efforts have proven that social vulnerability increases the rate of emergency medical incidents (Zottarelli et al. 2021).

This paper identifies spaces within an urban area that are most vulnerable to heat and where heat mitigation efforts can maximize benefits using Bexar County—home to San Antonio, Texas—as a case study. The study area is situated far to the south within the United States, see Fig. 1, within the humid subtropical (Cfa) Köppen-Geiger climate classification, bordering a hot semi-arid (BSh) zone (Beck et al. 2023). This shapes the magnitude and timing of local heat vulnerability. Summers are long, extremely hot, and often humid, with frequent heatwaves and prolonged periods of elevated nighttime temperatures that limit physiological recovery. Seasonal heat risk typically peaks from late spring through early fall, when both maximum and minimum temperatures are well above national averages. These conditions amplify health risks for vulnerable populations, particularly those with limited access to cooling resources (Boice et al. 2018). By situating San Antonio in this climatic context, the study's methods and results can be more readily understood and compared to regions experiencing similar hot, moisture-variable climates worldwide. Although only 13% of global land area, the humid subtropical classification hosts many large cities, including those in the southeastern U.S., much of eastern China and Japan, the eastern coast of Australia, most of Uruguay, and parts of Italy, France, Argentina, and Brazil. Therefore, large populations are exposed to a similar climate as the one studied here. Bexar County has a population of approximately 2 million, the sixteenth largest in the US (US Census Bureau 2021) and regularly has summer daily maximum temperatures above 100°F (38°C). Hundreds of heat-related illnesses are reported in Bexar County (City of San Antonio 2023) each year, and heat impact is not homogeneous across communities. This is particularly important in San Antonio, which has a very high Residential Income Segregation Index (RISI).

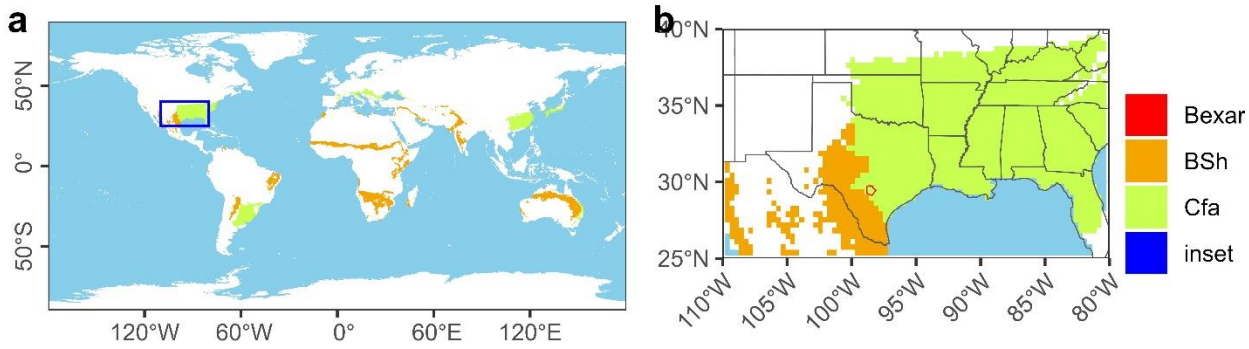

Figure 1 A map of (a) locations in the world with similar climate zones, adapted from Beck et al. (2023), and (b) an inset around the study area, highlighted in red, indicating its location in the southern part of the United States, not far (~200km) from the border with Mexico.

There is strong, scientific evidence for the adverse health impact of heat. In fact, "high non-optimal temperature" is a risk factor for the global burden of disease study (Murray et al. 2020). Hospitalizations increase during extreme heat for: cardiovascular disease, heat stroke, acute respiratory distress, hyperventilation, pulmonary stress, cognitive and organ dysfunction, and dehydration. These conditions can ultimately result in premature mortality (Anderson and Bell 2009; Nakamura and Aruga 2013; Li et al. 2015; Ebi et al. 2021a). However, current epidemiology primarily relies on temperature measured at the city or county scale, which is not sufficient for understanding the localized health impacts.

The urban heat island (UHI) effect (Stewart 2011; Shirani-bidabadi et al. 2019; Erdem et al. 2020; Wei et al. 2022) is well known, but the temperature variation is more complex than simply a rural-urban divide (Karimi et al. 2017). Several aspects of the urban environment contribute to the exacerbation of heat and ultimately the microclimate. Within an urban area, there is significant variation in characteristics of the built environment as well as local sources of heat and shade (Buyantuyev & Wu, 2009; Debbage & Shepherd, 2015; You et al., 2021). Therefore, exposure to heat varies even within the bounds of the UHI. The physical infrastructure consists of more impervious surfaces, many of which have dark color and reflectivity characteristics that exacerbate heat. In addition, anthropogenic waste heat creates additional sources of heat beyond the radiative energy balance driven by the sun and atmosphere. Additional investigation is needed to understand the effects of intra-urban heat islands (IUHI), locations with temperatures elevated further than the urban mean. While climate change is altering the temperature profiles of entire areas, urbanization processes often exacerbate the temperature change heterogeneously within urban areas by changing energy flow patterns through the absorption and retention of heat (Buyantuyev and Wu 2009; Erdem et al. 2020; You et al. 2021).

Due to the intra-urban variation in heat, efforts to reduce human exposure to heat should be targeted. Historically, data availability has not allowed for optimization of public investments at a very fine spatial resolution. In the existing paradigm, decisions were based on an incomplete picture, but the advances in technology and the data revolution can improve decision making to better serve residents. To close the gap, improvements in environmental data collection techniques have been used to allocate mitigation efforts in Chelsea, Massachusetts (Melaas et al. 2016; Chang et al. 2021; Milando et al. 2022) (a suburb of Boston), and Phoenix, Arizona

(Guhathakurta and Gober 2007; Gober et al. 2009, 2010). These prior efforts found that the ideal intervention might differ based on the characteristics of each neighborhood, which we have accounted for here through additional assessments beyond the level of heat exposure. As such, prioritization depends on the objective and city needs. Existing evaluations have often targeted occupational exposure (Sabrin et al. 2021; Alahmad et al. 2025), providing a strong basis upon which to expand. In the case of San Antonio, race, ethnicity, and income have been traditionally identified as major variables to define vulnerability (City of San Antonio 2019).

Using a vulnerability index is one approach to incorporate environmental justice into investigations of environmental hazards. Vulnerability indices can incorporate both physical exposure and the broader conditions of a person's life when quantifying the potential impact of an environmental hazard (Sabrin et al. 2022a). The goal of a vulnerability index is to simplify information from multiple data sources representing complex and interacting indicators and causes of vulnerability into an arrangement that is easy to understand and can be used in management decisions. In addition to helping decision makers identify vulnerable communities, these vulnerability indices can aid in the development or identification of appropriate interventions by providing insight into the factors causing the vulnerability. For example, a community that is vulnerable due to a high percentage of people with chronic disease may benefit from having better access to health care facilities while a low-income community with poorer housing conditions may benefit from infrastructure projects that reduce heat in the area.

Efforts have been made to do this in the U.S., including a national heat vulnerability index (ESRI 2018) that combines the Centers for Disease Control and Prevention (CDC) social vulnerability index with the National Oceanic and Atmospheric Administration (NOAA) projection of future heat events. Based on these efforts, Spielman et al. (2020) established that successful vulnerability metrics should be theoretically consistent, internally and externally consistent, practical, transparent, interpretable, and relevant. We build upon these efforts by evaluating a finer resolution and incorporating additional data sources to identify the areas that are already experiencing threats and thus at the most urgent risk.

To determine which neighborhoods are both particularly hot and particularly vulnerable to suffering negative health impacts of the heat, we developed a multi-faceted definition of vulnerability, building on prior work. (Xu et al. 2025) For example, Reid et al. (2009a) present an early heat vulnerability calculation showing that important factors include education, poverty, race, green space, social isolation, AC, and prevalence of elderly and diabetic residents. A similar version was used for New York state (Nayak et al. 2018). A recent commentary (Karanja et al. 2025) calls for optimized vulnerability assessments, specific to heat. We incorporate urban morphology as in Gong et al. (Gong et al. 2025) and similar to Guo et al. (2025) who used LCZ, surface temperature variation, and other indicators of exposure, vulnerability and adaptability to assess heat health risk inequality, however their adaptability characteristics may not be representative of accessibility in the US (Roy and Kar 2022).

In this study, we use a ranking system to identify priority neighborhoods for action. Vulnerability is determined through a combination of equity considerations and environmental characteristics. Through the use of a ranking system, we are able to combine a variety of disparate contributors to vulnerability into a single metric to identify priority areas for heat mitigation measures to be implemented.

Methods

Using the hazard-vulnerability-exposure definition of risk highlighted in the IPCC AR6 WGII (Ara Begum et al. 2022) we use a metric that incorporates the hazard (extreme heat) as well as the vulnerability and exposure. Vulnerability includes a lack of capacity to cope with extreme heat, which could be due to increased susceptibility due to health or a lack of resources. Exposure is defined by quantifying the degree to which an environmental hazard is present and identifying the occurrence of people in an area that could be adversely affected by the hazard. Exposure is represented by the fine scale assessment of variation in temperatures, as well as the presence of resources that can be used to avoid the heat.

Heat

Heat was assessed using remotely measured Land Surface Temperature (LST) data from the United States Geological Survey (USGS) Landsat missions, which provide 30x30m resolution data (Dwyer et al. 2018; Earth Resources Observation and Science (EROS) Center 2021; USGS 2023). This data enables a fine spatial scale understanding of the variation in thermal conditions. As clouds obscure the surface measurement, only measurements on clear sky days are included here and only measurements during the summer months (May-September) were considered. Heat data was based on measurements from May 20, 2022; May 28, 2022; June 29, 2022; July 7, 2022; September 9, 2022; June 16, 2023; June 24, 2023; July 10, 2023; July 18, 2023; August 11, 2023; August 27, 2023; September 20, 2023; August 21, 2024; and September 30, 2024.

When calculating the temperature variables, pixels identified as having any QA value other than 21824, indicating confident assessment of the pixel as having clear skies and not measuring water, ice, or clouds were removed. For cloud measurements, the averages include measurements from non-cloudy dates. For some lakes that are consistently covered in water, they are excluded from the analysis. This ensures that averages are accurately representing the heat island effect. For most of the measurements, the number of removed pixels is less than 1% of the 3.5 million available, and for May 20, 2022, July 7, 2022, and September 9, 2022 the removal rate was 6, 4, and 16%, respectively.

LST is correlated to near-surface air temperature, but typically higher. Surfaces absorb heat in different magnitudes and at different rates. Therefore, temperatures vary not only by location, but the rate at what they change through the day. While the relationship is complex, there is a positive correlation between LST and air temperature (Kloog et al. 2012; Rosenfeld et al. 2017). Therefore, it is reasonable to assume that there will be overlap in areas with high LST and high air temperature, and, by proxy, higher exposure to heat risk. LST is important data because it is the only thermal data that can provide a fine scale understanding of how thermal conditions vary across the urban area (Lopez Ochoa et al. 2024).

Examining the temperatures across multiple days is important to ensure that the results are consistent across dates. However, due to the different ranges of temperatures measured on different days, using the data directly is difficult. For this reason, we use the urban thermal field variance index (UTFVI) to normalize the data across the dates. The gridded data pixels from the satellite are saved as a raster file where each pixel (or cell) has its own temperature. UTFVI is a simple raster-based metric that calculates the percentage of thermal variance of a particular raster cell (i) with respect to the mean (average temperature) such as:

$$UTFVI_{i,d} = \frac{T_{i,d} - mean(\mathrm{T})_d}{mean(\mathrm{T})_d} \quad (1)$$

where $T_{i,d}$ is the temperature for a given pixel on a given day (d), and $mean(T)_d$ is the average temperature for all pixels on a given day. After calculating the UTFVI for each pixel for each day, an average UTFVI for each pixel was calculated. The average UTFVI across the 14 dates was then aggregated to the census block level to correspond with other data sets as in equation 2. The variation in heat (h_j) for a block can thus be calculated as

$$h_j = \frac{1}{N}\sum_{i \in j}\frac{1}{D}\sum_{d} UTFVI_{i,d} \quad (2)$$

where the index j represents the block, d represents the day of measurement, D represents the total number of measurement days included for each cell, and N is the number of cells included in the block. Calculations for averaging pixels (i) in each block (j) were performed with block level averages calculated using the extract function from the terra package (Hijmans 2020) for R based on census block definitions retrieved from the Tigris package (Walker 2015).

The relative heat variation is consistent across the analyzed dates. Each daily UTFVI for a block is highly significantly ($p < 0.001$) correlated with the overall average. The least correlated is on September 9, 2022 with a Pearson's correlation coefficient of 0.739 and 9 of the 14 dates have a coefficient greater than 0.9. This justifies the use of the average variation while also solidifying the justification for using this data to make infrastructure decisions by showing that the hottest areas are consistently injurious. The average UTFVI is plotted in Figure 2. From this figure, it is apparent that the urban center is typically warmer than the suburban areas toward the edges of the county, and that there are some cool areas even relatively near downtown. Also, the northern neighborhoods are cooler than southern neighborhoods.

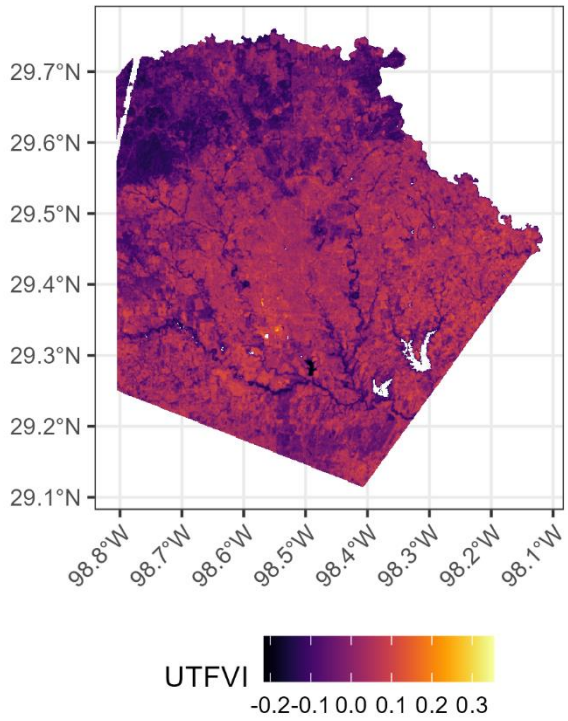

Figure 2 Average UTFVI in the original 30m resolution across 14 summer dates.

Equity

Although temperature variation is obviously an important factor in heat-related outcomes, vulnerability to heat can differ by population groups and communities (Niu et al. 2021; Cheng et al. 2021). We can refer to this as social vulnerability. The most relevant metrics for social vulnerability may vary, but previous research in San Antonio indicates that income, race, and ethnicity are important for understanding environmental justice in the study area (City of San Antonio, 2019; Gardner, 2022).

Income is related to the financial ability of individuals to cope with extreme weather. Higher income individuals may be more able to employ adaptations such as air conditioning or home improvements such as insulation. Median household income was used as the variable to represent income in each block group, which is the finest resolution at which this data is available. The median income for a census block group from the 2023 5-year ACS estimate is assigned to all census blocks within that group. For a census block group that does not have a median income reported, the median income at the tract level is assumed to apply.

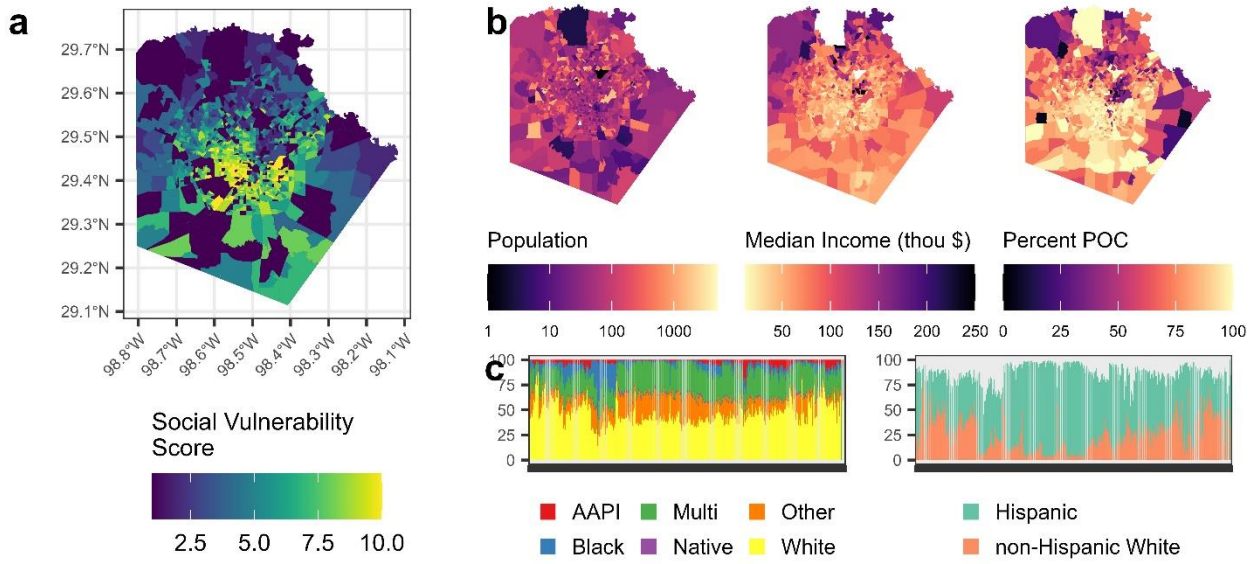

Figure 3 Distribution of (a) social vulnerability scores and (b) the underlying demographics. Higher scores indicate a more vulnerable population. Bar charts (c) show the demographic breakdowns across the city. AAPI includes "Asian alone" and "Native Hawaiian and Other Pacific Islander alone", "Native" includes "American Indian and Alaska Native alone" and "Multi" represents all multi-racial people.

Race and ethnicity help identify neighborhoods that have been historically under-resourced due to prior policies. In the U.S., redlining policies in the 1930s led to generational effects of segregation and disinvestment in areas with a large proportion of African American and Hispanic populations (Lee et al. 2022), and San Antonio is no exception. The heat-related concerns in San Antonio are also known to be higher in historically redlined areas (Li et al. 2022). In this work, race/ethnicity was treated as a binary considering the percentage of people reporting something other than non-Hispanic White at the block level based on the 2020 decennial census. While this is a simplification, it allows for consideration of environmental justice within a simple scoring framework that is designed to be easily communicated to local decision makers.

These variables were ranked as described below and the aggregate scores are plotted in Figure 3. Note that scores of 1 indicate no residential population, but people may still be exposed in those areas during recreational or occupational activities.

Ranking scores

To incorporate several sets of data using a range of units, each dataset was converted to a set of rankings. In each set of rankings, the higher values indicate an increase in potential vulnerability to heat (not necessarily a higher amount of the quantity ostensibly being represented). All data was treated at the block level for consistency in identification of regions across metrics.

For each metric, the distribution of values was calculated, and an approximately equal number of blocks assigned to each of a set of scores, as illustrated in Figure 4. This builds upon prior work in developing the Equity Atlas for the City of San Antonio (Gardner 2022) in which variables are assigned to quintiles and assigned 1-5 scores depending on where they fall in the distribution. Then, scores were added to the index using an equal weights scheme. Considering the high spatial variability of heat, a finer level of resolution is used. To calculate the rankings from the thermal variance distributions, percentiles of h_j were calculated in 10% increments, to create 10 ranked categories with scores from 1 to 10. Each block was assigned a value H_j from 1-10 based on the quantile of temperature, with 10 indicating the hottest temperatures. Race/ethnicity and income scores were calculated on a 1-5 basis with 20% increments (Fig 4 b,c) and summed as in eq. 3. Higher scores indicate a lower, and therefore more vulnerable, income and a higher proportion of the population identifying as something other than non-Hispanic, white. As the heat variation is the primary driver of this investigation, a finer distinction was considered for that metric. This also ensures that there is equal weighting between temperature and the total social metric, which considers the sum of two rankings. Summed scores range from 2-10, and blocks with no population, and therefore no income, race or ethnicity, are assigned a score of 1.

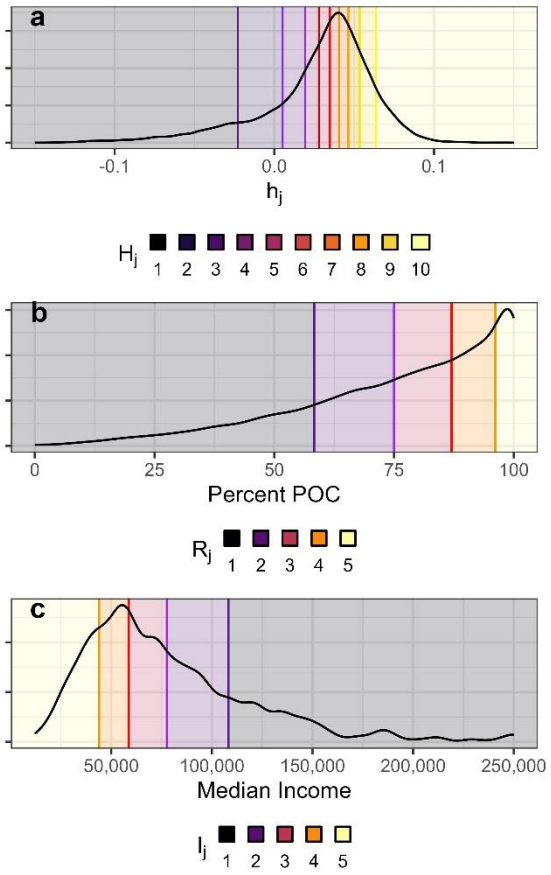

Figure 4 The distribution of block level thermal variance, h_j, and social characteristics is plotted in black and associated with the corresponding quantile-based score.

$$S_j = \begin{cases} 1, & P_j = 0 \\ I_j + R_j, & P_j > 0 \end{cases} \quad (3)$$

where S_j is the social score for block j, P is the population, I is the income ranking, and R is the race and ethnicity ranking. This score, combined with the heat score, H_j, determines the overall vulnerability score, V_j, which is represented by integer values between 2 and 10.

$$V_j = H_j + S_j \quad (4)$$

By using an aligned scoring system for the disparate metrics, an overall vulnerability can be determined through adding the scores. Therefore, overall vulnerability to heat can be represented by a composite score that is the sum of the heat scores and the social vulnerability scores. This helps quickly identify areas that are both particularly hot and where residents may be particularly vulnerable to succumbing to heat related illnesses.

Auxiliary Characteristics

Although temperature, income, race, and ethnicity were identified as the most relevant factors, they are not the only contributors to vulnerability. The included metrics were chosen based on prior work (Reid et al. 2009b; Li et al. 2015; Gardner 2022; Sabrin et al. 2022b) showing their relevance as well as a desire to pinpoint heavily affected areas. Many of the factors relevant to heat vulnerability are available only at the census tract or county level, which cover much larger areas. However, many of these coarser data are correlated with the variables we have included. To verify that appropriate factors were selected, we compared our composite index to other relative characteristics.

Metrics of health that were considered include the prevalence of pre-existing health conditions, specifically the prevalence of high cholesterol among adults who have been screened within the last 5 years, chronic obstructive pulmonary disease (COPD) prevalence among adults, stroke history among adults, and current asthma among adults. These data were obtained at the Census Tract level from the CDC Places data. (CDC 2023) Energy burden, the ratio of energy bills to income, represents the household's ability to afford increased energy costs associated with air conditioning. This was considered as this affects the ability of residents to avoid heat exposure. If the vulnerability ranking calculated here represents these additional vulnerability characteristics well, that indicates that the metric likely captures a wider range of vulnerability than what is explicitly included.

These additional metrics were evaluated using the ranking procedure described above. The pre-existing condition and energy burden data was only available at the census tract level. Each of these were assigned to 5 quantiles. Due to the mismatch in spatial resolution, a direct comparison with the vulnerability scores was not possible. However, due to interest in these well-known metrics, we assigned the maximum value of the overall vulnerability score found within a tract to that tract for comparison.

Local climate zones (LCZ)

Local climate zones (LCZ) (Stewart and Oke 2012) were used to determine whether the physical structure of different parts of the city has a measurable influence on heat vulnerability. We utilized the World Urban Database and Access Portal Tools (WUDAPT) Level 0 LCZ dataset for San Antonio, which was generated via the LCZ Generator platform (Demuzere et al. 2020, 2021). The dataset is based on the representative date of July 12, 2024, and follows the standardized WUDAPT protocol. The LCZ classification map is generated using remote sensing inputs, primarily derived from public datasets such as Landsat and SRTM with spatial resolutions of 30 to 90 meters, including NDVI, NDBI, land surface temperature, building height, and other features. LCZ classification was performed using 251 manually labeled training areas and remote sensing-based feature inputs with a spatial resolution 90 meters, combined through machine learning method. The resulting LCZ map achieved an overall accuracy of 0.72, while weighted

accuracy metrics reached up to 0.93, indicating a high level of classification reliability. This process supports a detailed spatial understanding of urban thermal characteristics and serves as a foundation for further analyses. Subsequent spatial analysis was conducted in ArcGIS pro, to identify the dominant LCZ type within each block using a majority rule approach. This method effectively identifies the dominant Local Climate Zone type for most blocks. However, for certain smaller blocks, the spatial extent may span across multiple LCZ classes with similar proportions, preventing any single class from attaining a clear majority. As a result, when no LCZ type accounts for more than 50% of the pixels within a block, no dominant LCZ can be assigned. Given the mismatch between the raster resolution (90*90m) and the small spatial scale of some blocks, we designated such cases as LCZ=0 to clearly mark them as having no definitive classification for further analysis. The LCZ at the block level are plotted in Figure 5 and are quantified in Table 1. The most common LCZ in the study area is “open lowrise”, which comprises 66% of the blocks in the county. Other common zones are “scattered trees” and “open midrise”, which each represent another 6% of the blocks, and “paved” which makes up another 5% of the county. Nine percent of the blocks were unable to be categorized at the block level using the methodology.

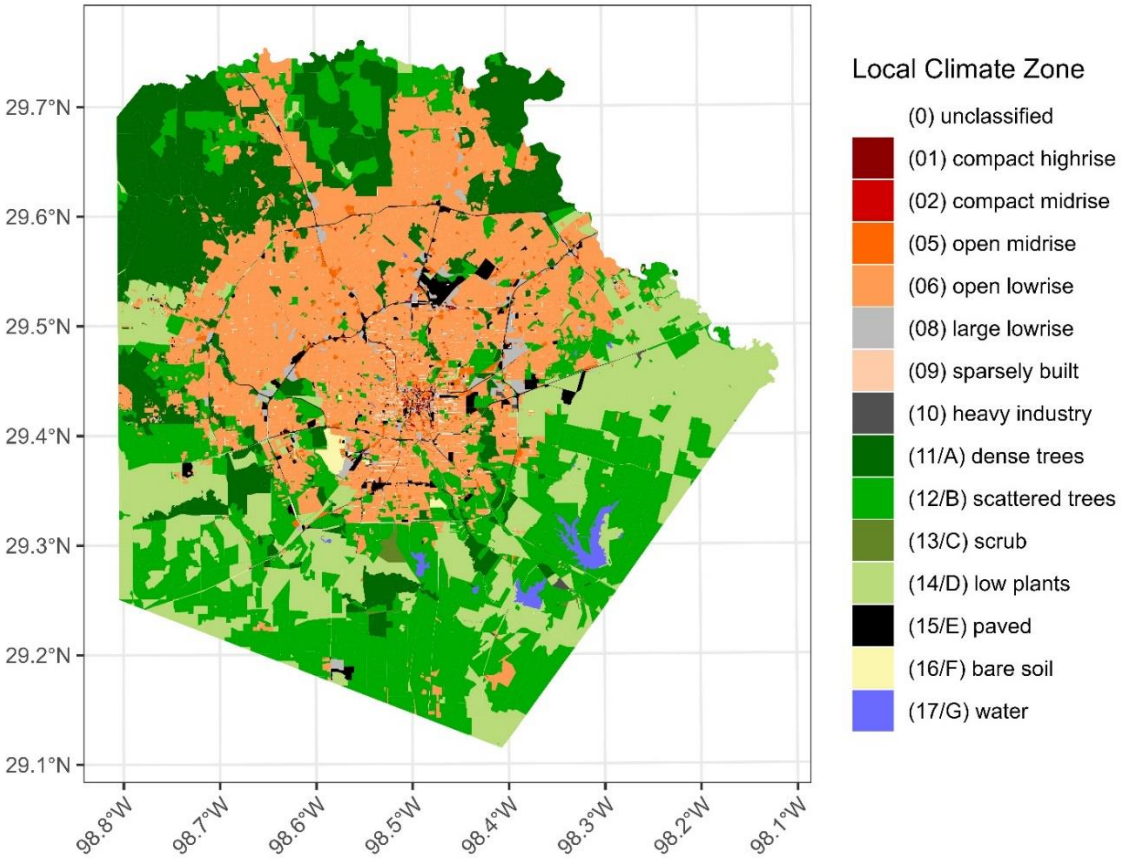

Figure 5 Identified Local Climate Zones in the study area, aggregated to the US Census block.

Results and Discussion

Considering the base vulnerability score that accounts for heat, income, race, and ethnicity, of the 23,695 census blocks in Bexar County, 175 of them (representing 14,989 residents) have the highest possible ranking of 20, meaning they are in the hottest 10% of all blocks, the lowest 20% of median income block groups, and the 20% of blocks with the highest proportion of residents of color. Another 489 blocks (population 37,376) have the second highest ranking of 19, and 854 (75,050 people) have a ranking of 18. Compared to the County population of 2,009,324, a much more targeted approach can treat these locations. The composite score for each block is plotted in Figure 6.

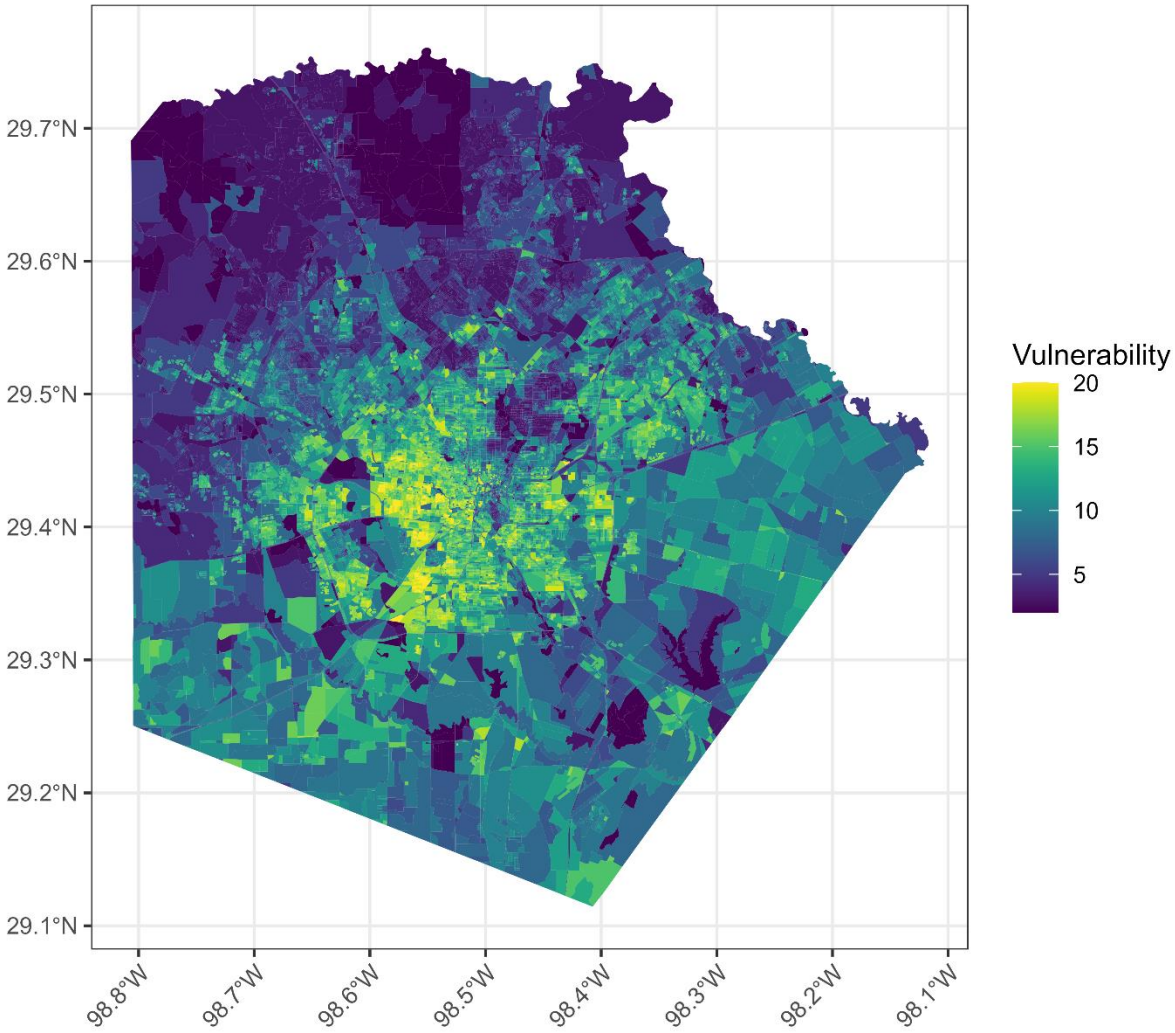

Figure 6 A map of the study area colored according to the composite vulnerability score, in which higher scores indicate more vulnerability to heat.

LCZ

As most heat mitigations are alterations to the physical environment, understanding the current state of the physical environment is important, particularly in the neighborhoods already

identified as vulnerable. Well known relationships between heat and urban form are seen in this study and visualized in Figure 7 and quantified in Table 1.

From Figure 7, it is clear that trees are associated with cooler blocks, as nearly all “dense tree” locations are in the lowest heat score area, and the “scattered tree” blocks are much more common in lower scoring areas. Water is also always much cooler than other areas, as is well established. Open midrise, large lowrise, and mixed built, are all more heavily represented in the hotter areas. Paved blocks are also more frequently higher scoring, although somewhat surprisingly some highly paved blocks appear even in moderate scoring areas. This is likely an albedo effect as the low scoring paved blocks are primarily highway interchanges and older parking lots that are lighter in color. The most common zone type in the study area (open lowrise) does not appear to be correlated to heat scores, suggesting its widespread presence doesn't necessarily contribute to or alleviate heat as significantly as other LCZ types. The unassigned (0) LCZ areas do not show a relationship to heat scores either, although they are less common at the extremes. This is likely due to the mitigating effects of multiple features.

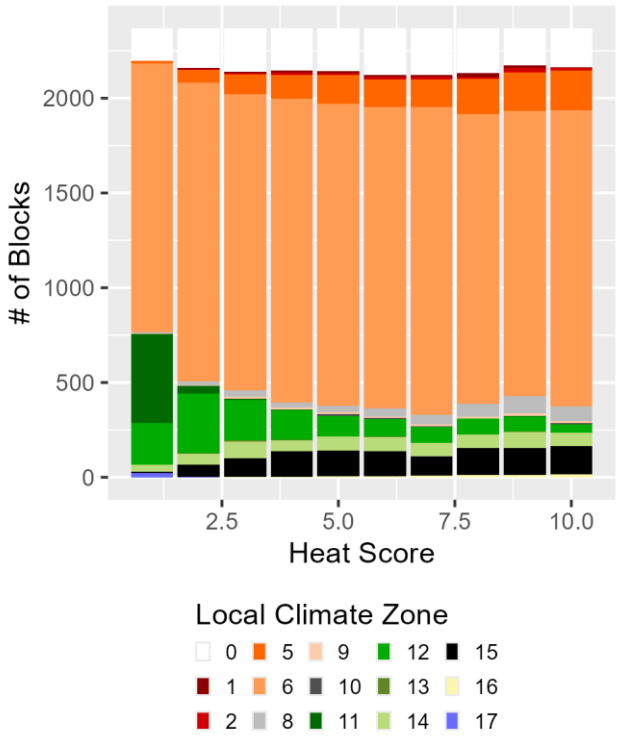

Figure 7 Each census block is categorized by LCZ as well as heat, confirming some patterns between LCZ and temperature. For the full name of each zone in the legend, see Table 1 or Figure 5.

An examination of Figure 7 shows a complex relationship between urban land cover and heat distribution, where the most prevalent landscapes are not always the coolest. The data illustrates that while the "open lowrise" environment contains the largest number of hot city blocks, this is primarily a function its sheer dominance across the study area. The role of greenery in heat mitigation proves to be nuanced, underscoring that not all green infrastructure provides equal benefits. Dense Trees are exceptionally effective at cooling, with an overwhelming majority of these areas registering the lowest possible heat score. This is attributable to extensive shade canopies and high rates of evapotranspiration. In contrast, other common green landscapes like scattered trees and low plants offer more moderate or even minimal cooling. Scattered trees create a mosaic of hot and cool spots, resulting in a wide distribution of heat scores, while low-lying plants and scrub provide little shade and are far less effective at reducing ambient temperatures. Other characteristics of the built environment are powerful drivers of urban heat. For example, the Paved category exhibits some of the highest heat scores, highlighting the impact of heat-absorbing materials like asphalt and the generation of anthropogenic waste heat from vehicles. Similarly, the Compact Highrise and Compact Midrise zones trend towards hotter temperatures, as their dense building formations can trap heat and obstruct airflow.

Comparing the composite score to LCZ, the reliance on residential location changes the picture. Predominantly paved areas are typically unoccupied, but not living on pavement doesn't mean it doesn't affect you. This is also true for heavy industry and compact high rise zones. Many of these are work places, where occupants may be exposed for 40 hours each week. Also, it is clear that trees and other plants are inversely related to socially vulnerable neighborhoods. While they provide cooling benefits to the neighborhoods where they are located, creating a more equitable distribution will help with both factors of the metric.

Table 1 The distribution of LCZ across Bexar county and the relationship with vulnerability.

	Entire County		*Composite Score > 17*		*Percent of LCZ scoring > 17*	
Local Climate Zone	**Blocks**	**Population**	**Blocks**	**Population**	**Blocks**	**Population**
(0) unclassified	2,190	38,597	127	4,723	6%	12%
(01) compact highrise	97	1,986	2	48	2%	2%
(02) compact midrise	104	8,047	9	3,458	9%	43%
(05) open midrise	1,360	81,118	110	8,633	8%	11%
(06) open lowrise	15,555	1,634,303	1,182	103,467	8%	6%
(08) large lowrise	454	16,855	17	2,752	4%	16%
(09) sparsely built	82	1,735	3	91	4%	5%
(10) heavy industry	31	177	-	-		
(11/A) dense trees	523	48,016	2	237	0%	0%
(12/B) scattered trees	1,391	122,947	25	1,557	2%	1%
(13/C) scrub	24	450	1	15	4%	3%
(14/D) low plants	684	38,880	5	428	1%	1%
(15/E) paved	1,110	15,861	34	1,947	3%	12%
(16/F) bare soil	64	352	1	59	2%	17%
(17/G) water	26	-	-	-		
Grand Total	***23,695***	***2,009,324***	***1,518***	***127,415***	***6%***	***6%***

The most prevalent zone type in the county is open lowrise (LCZ 6)**,** accounting for a significant 15,555 blocks and encompassing over 1.6 million residents. This category is highly representative of many residential neighborhoods and commercial areas across the study region. Interestingly, for open lowrise blocks, the distribution of composite scores spans the entire spectrum, with 7.6% of these blocks (1,182 blocks, affecting 6.3% of the population within this zone) scoring above 17. This suggests that while widespread, open lowrise areas don't inherently predispose a block to extreme heat, but rather may be influenced by localized factors not captured solely by the LCZ designation.

However, certain local climate types do exhibit a more direct relationship with composite scores. Blocks characterized by trees, particularly dense trees (LCZ 11/A), are consistently much cooler than other zones. Only 0.4% of dense tree blocks (2 blocks) score above 17, impacting a mere 0.5% of the population within this LCZ, highlighting their exceptional cooling value, but also the relationship between dense trees and higher resourced neighborhoods. Similarly, scattered trees also demonstrate this effect, with only 1.8% (25 blocks) scoring above 17. This robust

association between tree cover and heat scores underscores the critical role of urban forestry in heat mitigation strategies.

Other Metrics

Comparing the identified hot spots to other metrics helps validate that the heat metrics used are appropriate. Heat is concerning due to its consequences on health, so we have compared our identified vulnerable locations to those with health vulnerabilities. This data is available at the tract level from the CDC Places data, which is a much coarser resolution than the data used here. However, we can identify co-located vulnerabilities. Of the 70 tracts with the highest prevalence of high blood pressure (greater than 36%), 26 have blocks ranking in the highest vulnerability score and 54 of the tracts have scores above 17. Similarly, for the 76 tracts with the highest COPD prevalence among adults (above 7.7%), 26 have blocks with composite scores of 20 and 63 have blocks with composite scores above 17. Of the 74 tracts with the highest rate of diabetes (greater than 16.9%), 31 have the highest vulnerability score and 69 have scores above 17. These health statuses are associated with health outcomes relevant for heat (Ebi et al. 2021b). These and additional overlapping tract scores are shown in Figure (a).

Similar to the health conditions, energy burden aligns well with the identified vulnerabilities. Of the 70 tracts that have an energy burden above 7% (the top quintile), 25 rank in the highest vulnerability score, and 63 have blocks with scores above 17. As energy burden is a function of income, and may be affected by heat it is reasonable that there should be a very high overlap between these identifications. Due to the distribution of the tract level scores (See Figure c) a cubic splines fit was used. The fit parameters for these parameters with the tract level scores are shown in Table 2, with two example fits shown in Figure (b).

Table 2 Fit parameters between the tract level vulnerability scores and other tract level parameters.

	R^2	p
Obesity	0.6105	< 2e-16
General Health	0.6071	< 2e-16
Disability	0.5833	< 2e-16
Asthma	0.5125	< 2e-16
Diabetes	0.4689	< 2e-16
Energy Burden	0.4457	< 2e-16
COPD	0.3477	< 2e-16
Stroke	0.3411	< 2e-16
High blood pressure	0.209	< 2e-16
High cholesterol	0.05973	1.08E-13

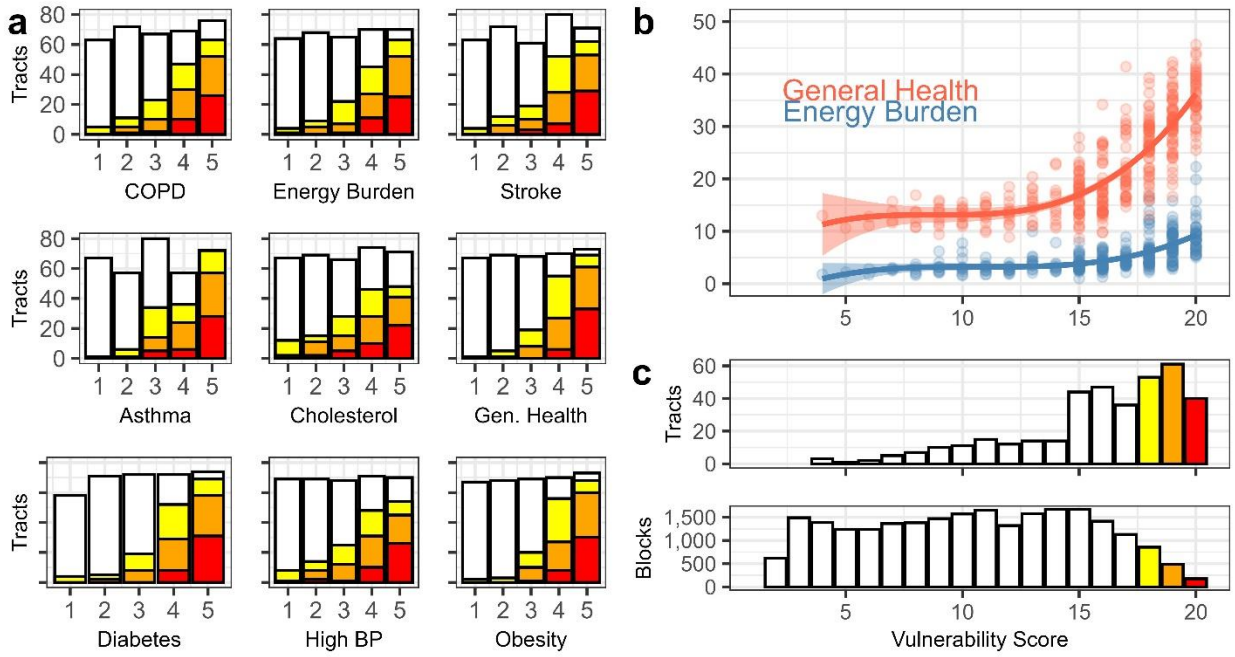

Figure 8 Comparison of the vulnerability score here and tract level metrics. Tract level scores are compared in (a) to similar tract level scoring of other metrics with colors corresponding to the vulnerability score bar charts in (c). The correlation of the tract level vulnerability and the tract level health and energy burden data are shown in (b).While energy burden and medical status are not expected to be perfectly correlated with heat vulnerability, these are factors that could also be included in a heat vulnerability index. By showing that the metrics included have already captured much of this additional vulnerability, it validates the choice of factors included within the index presented here.

We can further validate the vulnerability index by comparing it against others from the literature. Previous studies have created accurate, but intricate, measures of extreme heat and vulnerability (Johnson et al. 2012; Assaf and Assaad 2024), but decision makers often lack the technical capacity to work with such metrics. Cities often prefer more accessible metrics of vulnerability (Barron et al. 2018; Bu et al. 2024). We compare our index to some of these previous metrics. The Social Vulnerability Index (Centers for Disease Control and Prevention et al. 2022) is another tract level metric for which our index captures similar patterns. The correlation between the SVI and our index is 0.78 with a p-value less than $2.2x10^{-16}$. is Using the same cubic splines fitting process and tract level scoring as for the chronic health data, these two metrics have an R^2 of 0.6236 with a highly significant (< 2e-16) p-value. This index was also assessed for the City of Pheonix and found to have a correlation of 0.42 with their heat vulnerability index (Watkins et al. 2021).

Limitations

While useful, this study is not without limitations. First, while LST is strongly correlated with near-surface air temperature, it is not the same thing. LST is measured remotely by satellites and represents the temperature of the land's surface, which is typically higher than the air temperature. The relationship between LST and air temperature is complex, and the LST used here doesn't account for how surfaces absorb heat at different rates throughout the day. However,

LST is a valuable dataset because it provides a fine-scale understanding of thermal variations across an urban area that other thermal data cannot. While ground based monitors provide many relevant exposure metrics, they cannot provide the spatial resolution available from remote sensing products. A preliminary comparison between some ground-based temperature measurements is shown in **Error! Reference source not found.**, which indicates that the air temperature relative to the other sites is similar to the UTFVI for the same census blocks. The boxplots show the relative LST in that census block (with the UTFVI for each day multiplied by 100 and centered around 85) used to calculate h_j. The coolest location, which has a heat score, H_j, of 2, is consistently the coolest, while the warmest location is hotter than the middle location at some points in time and cooler at others. The hottest location has a heat score of 9 and the middle location has a score of 5. These preliminary comparisons show similar results to prior work that more explicitly validates the correlation of LST and air temperature (Cao et al. 2021; Amani-Beni et al. 2022).

Second, the LCZ classification had some limitations. Due to a mismatch between the raster resolution (90x90m) and the small size of some census blocks, some blocks were designated as having no definitive classification. Additionally, the study's social vulnerability metrics were a simplification of complex social factors. For example, race and ethnicity were treated as a binary variable, classifying individuals as either "non-Hispanic White" or "other". While this approach simplifies communication to local decision-makers, it may oversimplify the nuances of environmental justice. This classification was based on variables previously noted to be highly useful for the study area, but applying the index to alternative locations may require thoughtful assessment of the most appropriate social factors. The study also acknowledges that its heat vulnerability index focuses on residents' exposure to heat at their homes, which may not capture all exposure. For example, many of the hottest areas identified in the study are industrial zones or paved areas that have no population but are workplaces where occupants may be exposed to high heat for 40 hours per week.

Future research should expand on the findings of this study by investigating additional factors that contribute to heat vulnerability. While the current index focuses on heat, income, race, and ethnicity, other variables could be included, such as the history of redlining, medical access, housing quality, age, education, and nutrition. The current definition of minority populations could also be reallocated to a more detailed metric. To better capture residents' capacity to cope with heat, future work could incorporate data on housing conditions that promote climate adaptation, as well as vehicle ownership or public transit access, which may provide additional ways for people to escape the heat. Furthermore, future research could use data sources that better capture heat exposure beyond residential locations, such as incorporating data on where people work or spend recreational time.

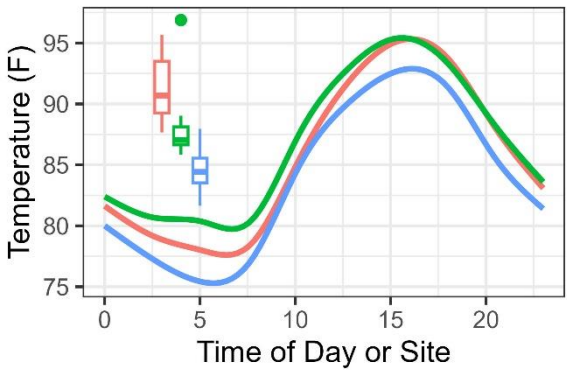

Figure 9 Lines plot the daily air temperature for three locations in the study area during summer 2025, and boxplots represent the UTFVI at the corresponding locations.

Conclusions

This scoring system has developed a roadmap for addressing vulnerabilities that account for the needs of the community under consideration. This analysis successfully improved heat mitigation implementation in 2025, resulting in heat resilience projects being deployed in the vulnerable areas shown in Figure 10. The findings were shared with the City of San Antonio government to enhance their operations. The local government then shared the information with the larger community through outreach events and an online StoryMap. Houses in neighborhoods identified as particularly vulnerable were improved through the installation of cool roofs based on characteristics of individual structures, and tree planting is ongoing in those neighborhoods. Longer term projects include adding shade structures around vulnerable areas. The easily interpretable vulnerability metric was key to rapid implementation of projects. Census blocks with scores greater than 17 were presented to the leaders of governmental offices, who chose to focus their efforts in portions of the city with dense clusters of these highly vulnerable areas. Developing an index with high spatial resolution was key to enabling active mitigation efforts as the capacity to execute change within a given year is limited and a smaller, targeted area can more easily be tackled within a planning period.

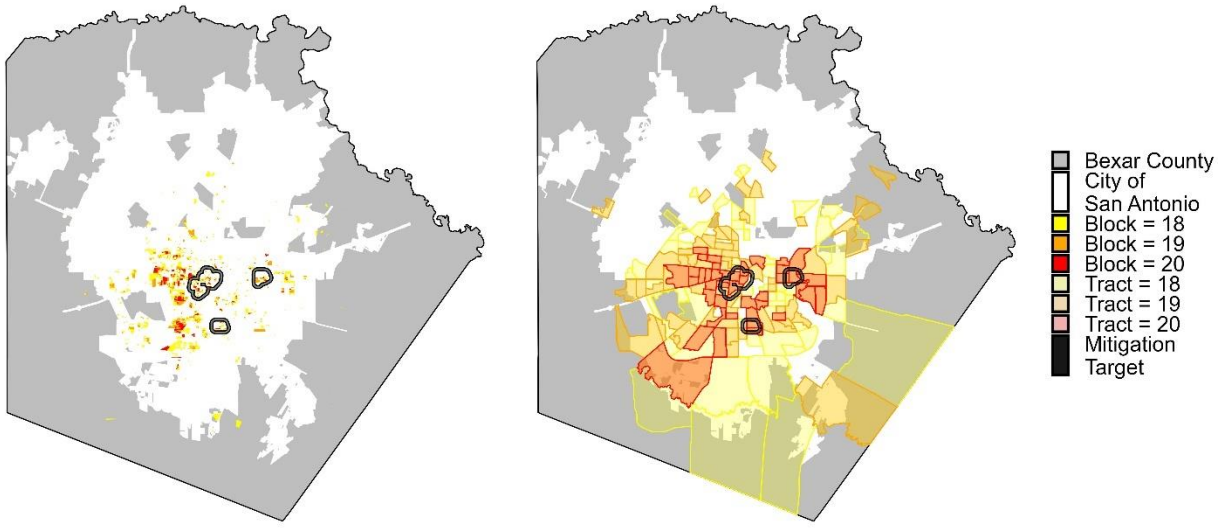

Figure 10 Maps show the most vulnerable locations in the study area and highlight where targeted heat mitigation efforts are being carried out by the City of San Antonio.

Considering a multifaceted definition of vulnerability helps improve the accuracy with which heat mitigation efforts can be targeted. For example, there are 23 blocks with a maximum heat score and an equity score of 2, the lowest populated score. While these should be examined to determine the cause of the heat, they may not be the first priority for mitigation. Another 449 blocks have the highest heat score, but no population. They should be examined to ensure they are not locations such as parks that may lead to high exposure, but may not be the most relevant for human health. Similarly, there are 35 blocks that score in the highest category for social vulnerability that have heat scores of 1 or 2 out of 10. While these neighborhoods may be in need of other interventions, heat is not the primary concern in these areas.

Figure 7 and Table 1 reinforce well established relationships including that high density (LCZ 01 and 02) is correlated with higher temperatures and green infrastructure (11-14/A-D) can help lower temperatures. It also confirms that water (17/G) has significantly cooler surface temperatures than land. This analysis shows that additional factors are needed to describe the interaction of urban environments with temperature. The majority (66%) of San Antonio consists of open low rise (06) construction, which does not show a particularly strong relationship to heat. Thus, while LCZ can be useful as a first pass in determining how to address heat, more work is needed.

This process could be adapted and applied to other localities, thereby enhancing data-driven decision-making at the local level. Incorporation of local knowledge to determine whether the social and physical environmental variables used here are most important should be included. Additional factors that could be investigated include history of red-lining, medical access, housing quality, age, education, and nutrition. (Akinya et al., 2014; Arbury et al., 2016; Emerson et al., 2015; Goossens et al., 2021; Hodshire et al., 2022; Levy, 2021; Nguyen et al., 2014; Polonik et al., 2023; Wilson, 2020)

Possible further considerations of vulnerable populations would include reallocating the definition of minority populations as it was collapsed to a binary metric, incorporating considerations of housing conditions that would promote climate adaptation, or considering vehicle ownership or public transit access that might enable additional mechanisms to escape heat. This determination was designed to be replicable for other municipalities or regions and the output is intended to be easily communicated to decision makers that may not be environmental experts. Other future work could include data sources that capture exposure better than residence and comparing this equal-weight index with more complex to understand indices that combine spatial clustering techniques (e.g. Moran's I) with variable reduction and weight calculation techniques (e.g. Principal Component Analysis – PCA).

Acknowledgments

The authors appreciate the acceptance and use of these efforts by the government of the City of San Antonio, particularly the Office of Sustainability.

References

Alahmad B, Kessler W, Alwadi Y, et al (2025) A nationwide analysis of heat and workplace injuries in the United States. Environ Health 24:65. https://doi.org/10.1186/s12940-025-01231-1

Amani-Beni M, Chen Y, Vasileva M, et al (2022) Quantitative-spatial relationships between air and surface temperature, a proxy for microclimate studies in fine-scale intra-urban areas? Sustainable Cities and Society 77:103584. https://doi.org/10.1016/j.scs.2021.103584

Anderson BG, Bell ML (2009) Weather-related mortality: how heat, cold, and heat waves affect mortality in the United States. Epidemiology 20:205–213. https://doi.org/10.1097/EDE.0b013e318190ee08

Ara Begum R, Lempert R, Ali E, et al (2022) Chapter 1: Point of Departure and Key Concepts. In: Portner H-O, Roberts DC, Tignor M, et al. (eds) Climate Change 2022: Impacts,

Adaptation and Vulnerability. Cambridge University Press, Cambridge, UK and New York, NY, USA, pp 121–196

Assaf G, Assaad RH (2024) Development and Validation of a Heat Resilience Index: Measuring Communities Resilience to Extreme Heat Events. Journal of Urban Planning and Development 150:04024034. https://doi.org/10.1061/JUPDDM.UPENG-4646

Barron L, Ruggieri D, Branas C (2018) Assessing Vulnerability to Heat: A Geospatial Analysis for the City of Philadelphia. Urban Science 2:38. https://doi.org/10.3390/urbansci2020038

Beck HE, McVicar TR, Vergopolan N, et al (2023) High-resolution (1 km) Köppen-Geiger maps for 1901–2099 based on constrained CMIP6 projections. Sci Data 10:724. https://doi.org/10.1038/s41597-023-02549-6

Boice DC, Garza ME, Holmes SE (2018) The Urban Heat Island of San Antonio, Texas, from 1991 to 2010. Journal of Geography, Environment and Earth Science International 1–13. https://doi.org/10.9734/JGEESI/2018/43367

Bu S, Smith KL, Masoud F, Sheinbaum A (2024) Spatial distribution of heat vulnerability in Toronto, Canada. Urban Climate 54:101838. https://doi.org/10.1016/j.uclim.2024.101838

Buyantuyev A, Wu J (2009) Urban heat islands and landscape heterogeneity: linking spatiotemporal variations in surface temperatures to land-cover and socioeconomic patterns. Landscape ecology 25:17–33. https://doi.org/10.1007/s10980-009-9402-4

Cao J, Zhou W, Zheng Z, et al (2021) Within-city spatial and temporal heterogeneity of air temperature and its relationship with land surface temperature. Landscape and Urban Planning 206:103979. https://doi.org/10.1016/j.landurbplan.2020.103979

CDC (2023) PLACES: Local Data for Better Health, Census Tract Data 2023 release

Centers for Disease Control and Prevention, Geospatial Research, Analysis, and Services Program, Agency for Toxic Substances and Disease Registry (2022) CDC/ATSDR Social Vulnerability Index 2020 Database US. https://www.atsdr.cdc.gov/placeandhealth/svi/data_documentation_download.html. Accessed 19 Sep 2023

Chang Y, Xiao J, Li X, et al (2021) Exploring diurnal cycles of surface urban heat island intensity in Boston with land surface temperature data derived from GOES-R geostationary satellites. Science of The Total Environment 763:144224. https://doi.org/10.1016/j.scitotenv.2020.144224

Cheng W, Li D, Liu Z, Brown RD (2021) Approaches for identifying heat-vulnerable populations and locations: A systematic review. Science of The Total Environment 799:149417. https://doi.org/10.1016/j.scitotenv.2021.149417

City of San Antonio (2023) Health Data & Statistics: Heat-Related Illnesses & Deaths. https://www.sanantonio.gov/Health/News/HealthDataReports#237423063-heat-. Accessed 13 Jul 2023

City of San Antonio (2019) Equity Atlas. https://www.sanantonio.gov/Equity/Initiatives/Atlas. Accessed 3 Jan 2023

Debbage N, Shepherd JM (2015) The urban heat island effect and city contiguity. Computers, Environment and Urban Systems 54:181–194. https://doi.org/10.1016/j.compenvurbsys.2015.08.002

Demuzere M, Hankey S, Mills G, et al (2020) Combining expert and crowd-sourced training data to map urban form and functions for the continental US. Scientific Data 7:4874 Bytes. https://doi.org/10.1038/s41597-020-00605-z

Demuzere M, Kittner J, Bechtel B (2021) LCZ Generator: A Web Application to Create Local Climate Zone Maps. Front Environ Sci 9:637455. https://doi.org/10.3389/fenvs.2021.637455

Dwyer JL, Roy DP, Sauer B, et al (2018) Analysis Ready Data: Enabling Analysis of the Landsat Archive. Remote Sensing 10:1363. https://doi.org/10.3390/rs10091363

Earth Resources Observation and Science (EROS) Center (2021) Landsat 4-9 U.S. Analysis Ready Data, Collection 2

Ebi KL, Capon A, Berry P, et al (2021a) Hot weather and heat extremes: health risks. Lancet 398:698–708. https://doi.org/10.1016/S0140-6736(21)01208-3

Ebi KL, Capon A, Berry P, et al (2021b) Hot weather and heat extremes: health risks. The Lancet 398:698–708. https://doi.org/10.1016/S0140-6736(21)01208-3

Erdem U, Cubukcu KM, Sharifi A (2020) An analysis of urban form factors driving Urban Heat Island: the case of Izmir. Environment, development and sustainability 23:7835–7859. https://doi.org/10.1007/s10668-020-00950-4

ESRI (2018) Future Heat Events and Social Vulnerability Dahsboard. https://www.arcgis.com/home/item.html?id=cbd68d9887574a10bc89ea4efe2b8087. Accessed 19 Jan 2024

Gardner B (2022) The San Antonio Equity Atlas. In: Data Smart City Solutions. https://datasmart.ash.harvard.edu/san-antonio-equity-atlas. Accessed 30 Dec 2022

Georgescu M, Broadbent AM, Krayenhoff ES (2024) Quantifying the decrease in heat exposure through adaptation and mitigation in twenty-first-century US cities. Nat Cities 1:42–50. https://doi.org/10.1038/s44284-023-00001-9

Gober P, Brazel A, Quay R, et al (2009) Using Watered Landscapes to Manipulate Urban Heat Island Effects: How Much Water Will It Take to Cool Phoenix? Journal of the American Planning Association 76:109–121. https://doi.org/10.1080/01944360903433113

Gober P, Kirkwood CW, Balling RC, et al (2010) Water Planning Under Climatic Uncertainty in Phoenix: Why We Need a New Paradigm. Annals of the Association of American Geographers 100:356–372. https://doi.org/10.1080/00045601003595420

Gong F-Y, Yang Z, Deng S (2025) Fine-scale assessment of diurnal heat health risk based on satellite and street view images. Cities 162:105963. https://doi.org/10.1016/j.cities.2025.105963

Guhathakurta S, Gober P (2007) The Impact of the Phoenix Urban Heat Island on Residential Water Use. Journal of the American Planning Association 73:317–329. https://doi.org/10.1080/01944360708977980

Guo F, Fan G, Zhao J, et al (2025) Urban heat health risk inequality and its drivers based on local climate zones: A case study of Qingdao, China. Building and Environment 275:112827. https://doi.org/10.1016/j.buildenv.2025.112827

Hijmans RJ (2020) terra: Spatial Data Analysis. 1.8-54

Johnson DP, Stanforth A, Lulla V, Luber G (2012) Developing an applied extreme heat vulnerability index utilizing socioeconomic and environmental data. Applied Geography 35:23–31. https://doi.org/10.1016/j.apgeog.2012.04.006

Karanja J, Vanos J, Georgescu M, et al (2025) The Imperative for Hazard- and Place-Specific Assessment of Heat Vulnerability. Environmental Health Perspectives 133:055003. https://doi.org/10.1289/EHP14801

Karimi M, Vant-Hull B, Nazari R, et al (2017) Predicting surface temperature variation in urban settings using real-time weather forecasts. Urban Climate 20:192–201. https://doi.org/10.1016/j.uclim.2017.04.008

Khatana SAM, Werner RM, Groeneveld PW (2022) Association of Extreme Heat With All-Cause Mortality in the Contiguous US, 2008-2017. JAMA Network Open 5:e2212957. https://doi.org/10.1001/jamanetworkopen.2022.12957

Kloog I, Chudnovsky A, Koutrakis P, Schwartz J (2012) Temporal and spatial assessments of minimum air temperature using satellite surface temperature measurements in Massachusetts, USA. The Science of the total environment 432:85–92. https://doi.org/10.1016/j.scitotenv.2012.05.095

Lee EK, Donley G, Ciesielski TH, et al (2022) Health outcomes in redlined versus non-redlined neighborhoods: A systematic review and meta-analysis. Social Science & Medicine 294:114696. https://doi.org/10.1016/j.socscimed.2021.114696

Li D, Newman GD, Wilson B, et al (2022) Modeling the Relationships Between Historical Redlining, Urban Heat, and Heat-Related Emergency Department Visits: An Examination of 11 Texas Cities. Environ Plan B Urban Anal City Sci 49:933–952. https://doi.org/10.1177/23998083211039854

Li M, Gu S, Bi P, et al (2015) Heat Waves and Morbidity: Current Knowledge and Further Direction-A Comprehensive Literature Review. International Journal of Environmental Research and Public Health 12:5256–5283. https://doi.org/10.3390/ijerph120505256

Lopez Ochoa E, Brown KE, Lee RJ, Zhai W (2024) Quantifying the spatial aggregation bias of urban heat data. Urban Climate

Melaas EK, Wang JA, Miller DL, Friedl MA (2016) Interactions between urban vegetation and surface urban heat islands: a case study in the Boston metropolitan region. Environ Res Lett 11:054020. https://doi.org/10.1088/1748-9326/11/5/054020

Milando CW, Black-Ingersoll F, Heidari L, et al (2022) Mixed methods assessment of personal heat exposure, sleep, physical activity, and heat adaptation strategies among urban residents in the Boston area, MA. BMC Public Health 22:2314. https://doi.org/10.1186/s12889-022-14692-7

Murray CJL, Aravkin AY, Zheng P, et al (2020) Global burden of 87 risk factors in 204 countries and territories, 1990–2019: a systematic analysis for the Global Burden of Disease Study 2019. The Lancet 396:1223–1249. https://doi.org/10.1016/S0140-6736(20)30752-2

Nakamura S, Aruga T (2013) Epidemiology of Heat Illness. 56:

Nayak SG, Shrestha S, Kinney PL, et al (2018) Development of a heat vulnerability index for New York State. Public health (London) 161:127–137. https://doi.org/10.1016/j.puhe.2017.09.006

Niu Y, Li Z, Gao Y, et al (2021) A Systematic Review of the Development and Validation of the Heat Vulnerability Index: Major Factors, Methods, and Spatial Units. Current Climate Change Reports 7:87–97. https://doi.org/10.1007/s40641-021-00173-3

Reid CE, O'Neill MS, Gronlund CJ, et al (2009a) Mapping Community Determinants of Heat Vulnerability. Environmental health perspectives 117:1730–1736. https://doi.org/10.1289/ehp.0900683

Reid CE, O'Neill MS, Gronlund CJ, et al (2009b) Mapping Community Determinants of Heat Vulnerability. Environmental Health Perspectives 117:1730–1736. https://doi.org/10.1289/ehp.0900683

Rosenfeld A, Dorman M, Schwartz J, et al (2017) Estimating daily minimum, maximum, and mean near surface air temperature using hybrid satellite models across Israel. Environmental research 159:297–312. https://doi.org/10.1016/j.envres.2017.08.017

Roy A, Kar B (2022) A multicriteria decision analysis framework to measure equitable healthcare access during COVID-19. Journal of Transport & Health 24:101331. https://doi.org/10.1016/j.jth.2022.101331

Sabrin S, Karimi M, Nazari R (2022a) Modeling heat island exposure and vulnerability utilizing earth observations and social drivers: A case study for Alabama, USA. Building and Environment 226:109686. https://doi.org/10.1016/j.buildenv.2022.109686

Sabrin S, Karimi M, Nazari R (2022b) Modeling heat island exposure and vulnerability utilizing earth observations and social drivers: A case study for Alabama, USA. Building and Environment 226:109686. https://doi.org/10.1016/j.buildenv.2022.109686

Sabrin S, Zech WC, Nazari R, Karimi M (2021) Understanding occupational heat exposure in the United States and proposing a quantifying stress index. Int Arch Occup Environ Health 94:1983–2000. https://doi.org/10.1007/s00420-021-01711-0

Shirani-bidabadi N, Nasrabadi T, Faryadi S, et al (2019) Evaluating the spatial distribution and the intensity of urban heat island using remote sensing, case study of Isfahan city in Iran. Sustainable Cities and Society 45:686–692. https://doi.org/10.1016/j.scs.2018.12.005

Spielman SE, Tuccillo J, Folch DC, et al (2020) Evaluating social vulnerability indicators: criteria and their application to the Social Vulnerability Index. Nat Hazards 100:417–436. https://doi.org/10.1007/s11069-019-03820-z

Stewart ID (2011) A systematic review and scientific critique of methodology in modern urban heat island literature. International Journal of Climatology 31:200–217. https://doi.org/10.1002/joc.2141

Stewart ID, Oke TR (2012) Local Climate Zones for Urban Temperature Studies. https://doi.org/10.1175/BAMS-D-11-00019.1

US Census Bureau (2021) American Community Survey

USGS (2023) Landsat Collection 2 U.S. Analysis Ready Data

Walker K (2015) tigris: Load Census TIGER/Line Shapefiles. 2.2.1

Watkins LE, Wright MK, Kurtz LC, et al (2021) Extreme heat vulnerability in Phoenix, Arizona: A comparison of all-hazard and hazard-specific indices with household experiences. Applied Geography 131:102430. https://doi.org/10.1016/j.apgeog.2021.102430

Wei C, Chen W, Lu Y, et al (2022) Synergies between Urban Heat Island and Urban Heat Wave Effects in 9 Global Mega-Regions from 2003 to 2020. Remote Sensing 14:70. https://doi.org/10.3390/rs14010070

Xu C, Wei R, Tong H (2025) A Systematic Review of Methodological Advances in Urban Heatwave Risk Assessment: Integrating Multi-Source Data and Hybrid Weighting Methods. Sustainability 17:3747. https://doi.org/10.3390/su17083747

You M, Lai R, Lin J, Zhu Z (2021) Quantitative Analysis of a Spatial Distribution and Driving Factors of the Urban Heat Island Effect: A Case Study of Fuzhou Central Area, China. International journal of environmental research and public health 18:13088. https://doi.org/10.3390/ijerph182413088

Zottarelli LK, Sharif HO, Xu X, Sunil TS (2021) Effects of social vulnerability and heat index on emergency medical service incidents in San Antonio, Texas, in 2018. Journal of epidemiology and community health (1979) 75:271–276. https://doi.org/10.1136/jech-2019-213256